Excited states of trans-stilbene and 1,4-diphenylbutadiene

Near and vacuum UV polarization spectroscopy

Nguyen, Duy Duc; Jones, Nykola C.; Hoffmann, Søren Vrønning; Spanget-Larsen, Jens

Published in:
Journal of Molecular Structure

DOI:
10.1016/j.molstruc.2023.136206

Publication date:
2023

Document Version
Publisher's PDF, also known as Version of record

Citation for published version (APA):
Nguyen, D. D., Jones, N. C., Hoffmann, S. V., & Spanget-Larsen, J. (2023). Excited states of *trans*-stilbene and 1,4-diphenylbutadiene: Near and vacuum UV polarization spectroscopy. *Journal of Molecular Structure*, *1293*, Article 136206. https://doi.org/10.1016/j.molstruc.2023.136206

Journal of Molecular Structure 1293 (2023) 136206

Contents lists available at ScienceDirect

Journal of Molecular Structure

journal homepage: www.elsevier.com/locate/molstr

Excited states of *trans*-stilbene and 1,4-diphenylbutadiene. Near and vacuum UV polarization spectroscopy

Duy Duc Nguyen [a,1], Nykola C. Jones [b], Søren V. Hoffmann [b], Jens Spanget-Larsen [a,*]

[a] Department of Science and Environment, Roskilde University, Universitetsvej 1, Roskilde DK-4000, Denmark
[b] ISA, Department of Physics and Astronomy, Aarhus University, Ny Munkegade 120, Aarhus C DK-8000, Denmark

ARTICLE INFO

Keywords:
Linear Dichroism (LD)
Polarization spectroscopy
Near and vacuum UV
Synchrotron radiation
Stretched polyethylene
LCOAO and TD-DFT calculations

ABSTRACT

The UV absorbance spectra of *trans*-stilbene ((*E*)-1,2-diphenylethene, DPE) and (*E,E'*)-1,4-diphenyl-1,3-butadiene (DPB) are investigated by Synchrotron Radiation Linear Dichroism (SRLD) spectroscopy using stretched polyethylene as an anisotropic solvent. The investigation covers the range 58,000–25,000 cm^{-1} (172–400 nm). The observed polarization data provide information on the transition moment directions of the observed spectral features. The wavenumbers, intensities, and polarization directions of the observed spectral bands are compared with the results of quantum chemical calculations using the semiempirical all-valence-electrons method LCOAO and Time-Dependent Density Functional Theory (TD–DFT) with the functional CAM-B3LYP.

1. Introduction

The photochemical and photophysical properties of α,ω-diphenylpolyenes have been studied for decades [1,2]. The considerable interest in the photochemistry (*E/Z* photoisomerization) of these compounds may be attributed to their similarity to biologically important chromophores such as visual pigments (retinal) and carotenes [3]. Much effort has been devoted to studies of the two lowest excited electronic states, which in some environments appear to be nearly degenerate [4]. For recent investigations and entries to the literature, see Refs. [4–7].

In the present publication we report the results of a study of the electronic states of *trans*-stilbene ((*E*)−1,2-diphenylethene, DPE) and (*E, E'*)−1,4-diphenyl-1,3-butadiene (DPB) (Scheme 1), the first two members of the α,ω-diphenylpolyene series. Their absorbance spectra are investigated by UV Synchrotron Radiation Linear Dichroism (SRLD) spectroscopy on molecular samples aligned in stretched polyethylene (PE). With synchrotron radiation [8,9] the investigated spectral range can be extended to about 58,000 cm^{-1} (172 nm). The measured LD yields information on the polarization directions of the observed transitions [10–15].

The experimental energies, intensities, and polarization directions are compared with the results of theoretical calculations using the Linear Combination of Orthogonalized Atomic Orbitals (LCOAO) model [16, 17] and Time-Dependent Density Functional Theory (TD-DFT) [18–21] with the functional CAM-B3LYP [22]. The semiempirical all-valence-electrons LCOAO procedure was specifically developed for prediction of the electronic absorption and MCD [23] spectra of conjugated hydrocarbons [16,17] and is recommended for large π systems [18]. In a recent investigation [24], the combined results of LCOAO and TD–CAM-B3LYP calculations provided an adequate description of the related chromophore 1,4-distyrylbenzene (DSB, Scheme 1).

Additional information is provided as Supplementary data, referred to in the ensuing text as S1 - S12.

2. Experimental

2.1. Sample preparation

The hydrocarbons DPE [CAS 103–30–0] (97%) and DPB [CAS 538–81–8] (98%) were purchased from BDH Chemicals and Sigma-Aldrich, respectively. The spectroscopic purity of the substances was checked by comparison with reference spectra available online [25]. Low-density polyethylene (PE) was obtained from Hinnum Plast, Denmark, as pure 100 μm sheet material. PE samples with DPE and DPB for LD spectroscopy were produced in the following way: A piece of the PE sheet was submerged into a saturated solution of the hydrocarbon in chloroform (Merck Uvasol) at room temperature for several days.

* Corresponding author.
E-mail address: Spanget@ruc.dk (J. Spanget-Larsen).
[1] Present address: Duy Duc Nguyen, Intertek Vietnam Limited, Tan Binh District, Ho Chi Minh City, Vietnam.

https://doi.org/10.1016/j.molstruc.2023.136206
Received 22 May 2023; Accepted 13 July 2023
Available online 15 July 2023

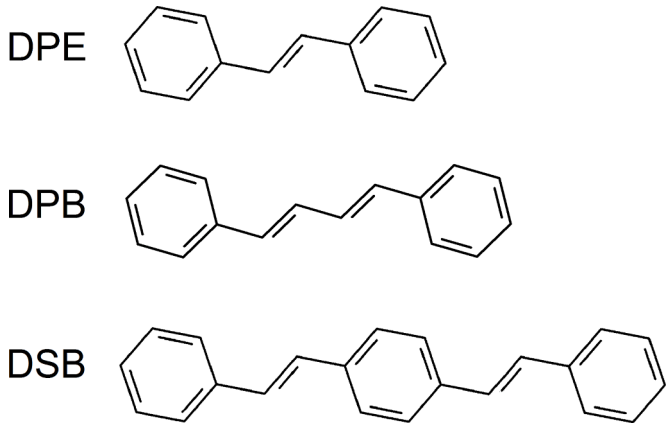

Scheme 1. (*E*)−1,2-diphenylethene (*trans*-stilbene, DPE), (*E,E'*)−1,4-diphenyl-1,3-butadiene (DPB), and 1,4-distyrylbenzene (DSB).

Subsequently, the chloroform was allowed to evaporate from the doped sample, and crystalline deposits on the surface were removed with methanol (Merck Uvasol). The PE sheet sample was finally uniaxially stretched by ca. 500%. Samples without solutes were prepared in the same manner for use as references. Further details on stretched PE samples can be found in the literature [10–15].

2.2. Linear dichroism (LD) spectroscopy

Synchrotron Radiation Linear Dichroism (SRLD) spectra of DPE and DPB were measured in the range 58,000–27,800 cm^{-1} (172–360 nm) on the CD1 beamline [8,9] at the storage ring ASTRID at the Centre for Storage Ring Facilities (ISA). The LD spectrum of DPB in the region 33,300–25,000 cm^{-1} (300–400 nm) was recorded on a UV-2101 PC Shimadzu spectrophotometer equipped with rotatable Glan-Taylor prism polarizers in both sample and reference beams. Two absorbance curves were recorded at room temperature with the electric vector of the sample beam parallel (U) and perpendicular (V) to the stretching direction of the PE sample. The observed baseline-corrected LD absorbance curves $E_U(\tilde{\nu})$ and $E_V(\tilde{\nu})$ are shown in Figs. 1 and 2; the curve $3E_{ISO}(\tilde{\nu}) = E_U(\tilde{\nu}) + 2E_V(\tilde{\nu})$ is three times the absorbance that would have been measured in an isotropic experiment on the same sample [10,11]. Wavenumbers and relative intensities of the main band systems *A, B, C*, and *D* for DPE and DPB are listed in Tables 1 and 2. A version of the observed spectra with indication of all peak wavenumbers and absorbances is provided in S1.

3. Calculational details

The electronic transitions of DPE and DPB were computed with the semiempirical all-valence-electrons method LCOAO [16,17] and with TD-DFT using the functional CAM-B3LYP [22]. The LCOAO calculations were performed with the computer program published in Ref. [26], the CAM-B3LYP calculations with the Gaussian 16 software package [27].

The LCOAO calculations included interaction between all singly excited singlet configurations generated by promotion of an electron from occupied π to unoccupied π* molecular orbitals (MOs), comprising 49 and 64 π-π*configurations for DPE and DPB, respectively. In addition to transition energies, intensities, and polarization directions, these calculations provided predictions of MCD B-terms [17,23] for the computed electronic transitions. The input geometries for the LCOAO calculations were taken as those optimized in the gas phase under the assumption of planar C_{2h} molecular symmetries with the B3LYP [28,29] density functional and the basis set cc-pVTZ [30,31], corresponding to the geometry adopted for DPB in a previous study [32]. The main transitions obtained with LCOAO are listed in Tables 1 and 2, complete listings of all LCOAO results are provided as S4 – S7.

CAM-B3LYP and TD–CAM-B3LYP calculations were carried out with the basis sets cc-pVTZ and AUG-cc-pVTZ (that is, without and with diffuse functions) [30,31]. The isotropic influence of the solvent was approximated by the Polarizable Continuum Model IEFPCM [33–36] using solvent = *n*-hexadecane [27]. Ground state C_{2h} molecular geometries were optimized with CAM-B3LYP with the respective basis sets, representing dispersion effects by the model by Grimme [37] (empiricaldispersion = gd3bj [27]). Frequency analyses (S9,S10) indicate that the molecular equilibrium geometries may deviate slightly from planarity. The stretched PE medium is known to exhibit a marked planarization effect for this class of molecules [38–41] and in the following, the DPE and DPB chromophores are described under the assumption of planar C_{2h} molecular symmetry. The TD–CAM-B3LYP calculations considered vertical transitions to the lowest 70 and 100 excited singlet states for DPE and DPB, respectively. Complete listings of all transitions computed with TD–CAM-B3LYP/AUG-cc-pVTZ are provided as S11 and S12.

4. Results and discussion

4.1. Linear dichroism: orientation factors and polarization directions

The observed LD absorption curves $E_U(\tilde{\nu})$ and $E_V(\tilde{\nu})$ are shown in Figs. 1 and 2 (top). For a uniaxial sample the curves can be written as [10–15]

$$E_U(\tilde{\nu}) = \sum_i K_i A_i(\tilde{\nu}) \tag{1}$$

$$E_V(\tilde{\nu}) = \sum_i \frac{1}{2}(1 - K_i)A_i(\tilde{\nu})$$

The sum is over all transitions i contributing to the observed spectrum, $A_i(\tilde{\nu})$ is the absorbance due to the i'th transition, and $K_i = \langle\cos^2(\boldsymbol{M}_i, U)\rangle$ is the orientation factor for this transition. Here $(\boldsymbol{M}_i, U)$ is the angle of the dipole moment vector $\boldsymbol{M}_i$ of transition i with the polymer stretching direction U [10–15]. The pointed brackets indicate the average over all solute molecules in the light path. A large orientation factor indicates that the transition moment is efficiently aligned with the stretching direction, and vice versa. We estimate the K_i values by considering the 'reduced' absorbance curves $r_K(\tilde{\nu}) = (1-K)E_U(\tilde{\nu}) - 2KE_V(\tilde{\nu})$ [12]. The contribution from transition i vanishes from the linear combination $r_K(\tilde{\nu})$ for $K = K_i$. If a spectral feature due to transition i can be identified in both $E_U(\tilde{\nu})$ and $E_V(\tilde{\nu})$, the K_i value may thus be determined by visual inspection [12]. Families of curves $r_K(\tilde{\nu})$ for DPE and DPB with K ranging between the limits 0 and 1 are shown in Figs. 1 and 2 (bottom). The orientation factors K for the observed absorbance bands are listed in Tables 1 and 2.

According to the C_{2h} molecular point group, dipole allowed transitions in DPE and DPB are either polarized along the molecular C_2 symmetry axis z or in the molecular x,y plane. We shall assume that the observed absorbance is primarily due to π−π* transitions and thus polarized in the molecular plane (this assumption is supported by the calculated results (S6,S7,S11,S12)). But infinite moment directions are possible for in-plane polarized transitions. We thus need to determine the angles ϕ_i formed by the moments of the observed transitions i with a specific, well-defined axis in the molecular plane. This axis is traditionally chosen as the "orientation axis" [10,11], the molecular axis x corresponding to the largest value of the average cosine squared, $\langle\cos^2(x, U)\rangle = K_x$, also called the "long axis" of the molecule. We shall assume that the orientation axes for DPE and DPB correspond to the longest molecular dimensions [32,43] as indicated in Scheme 2. The in-plane "short axis" y perpendicular to x corresponds to the lowest average cosine squared among directions in the plane, $\langle\cos^2(y, U)\rangle = K_y$ [10,11]. The C_2 symmetry axis z is perpendicular to x and y, and we have $K_x + K_y + K_z = 1$. For a transition i polarized in the molecular x,y plane, the

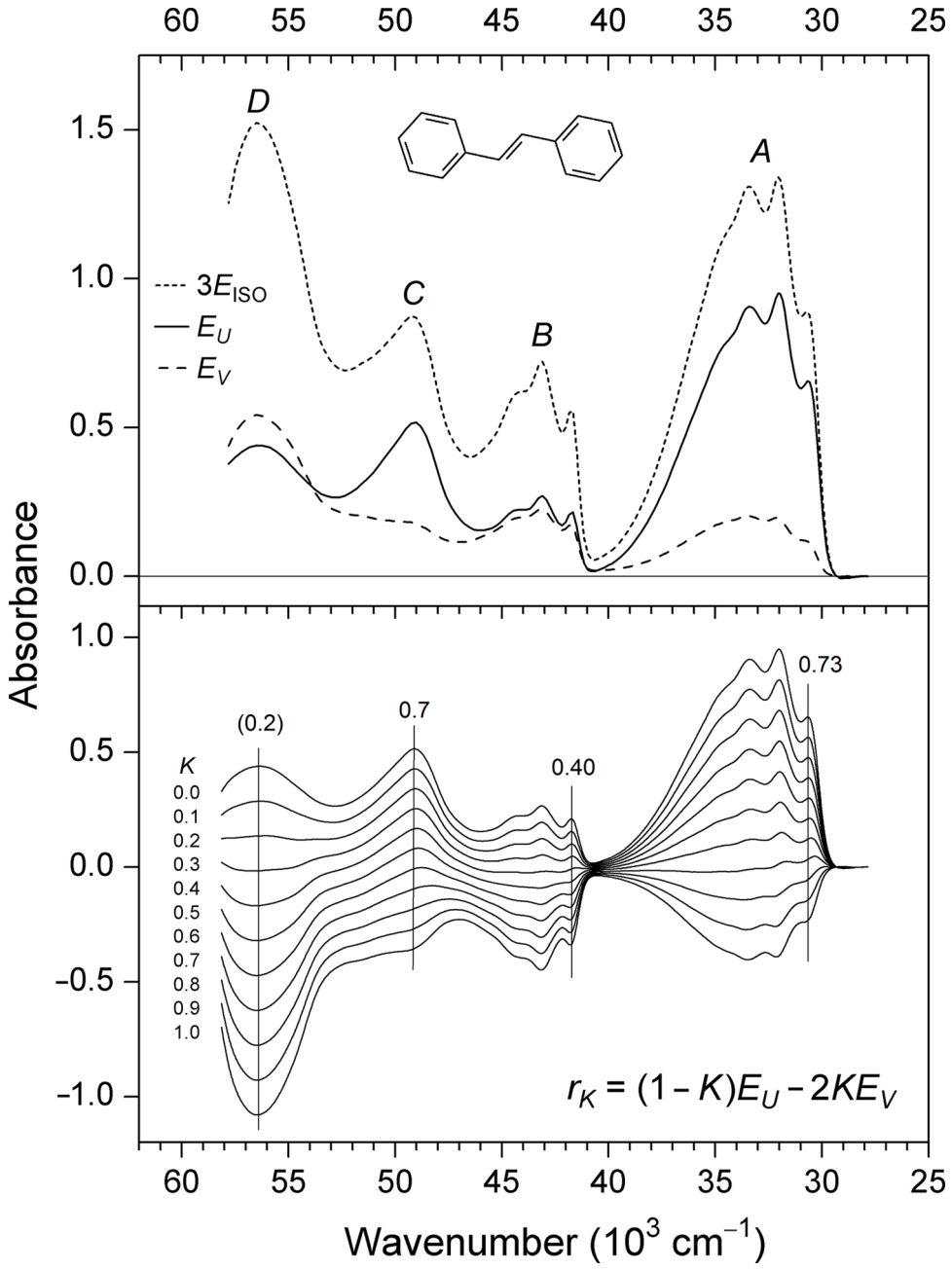

Fig. 1. *Top:* Linear Dichroism (LD) absorbance curves for DPE in stretched polyethylene. E_U and E_V indicate the absorbance curves measured with the stretching direction U parallel and perpendicular to the electric vector of the radiation. $3E_{ISO} = E_U + 2E_V$ is three times the absorbance that would have been measured in an isotropic experiment on the same sample. *Bottom:* Family of reduced absorbance curves $r_K = (1-K)E_U - 2KE_V$ with K varying from 0 to 1 in steps of 0.1.

following relation holds [10]:

$$|\phi_i| = \tan^{-1}\sqrt{(K_x - K_i)/(K_i - K_y)} \qquad (2)$$

Provided the orientation factors K_x and K_y for the in-plane axes x and y can be derived, the numerical values of the individual transition moment angles ϕ_i can thus be estimated from the observed K_i values.

4.1.1. Transition moment angles for DPE

Tanizaki et al. [42], Uznanski et al. [43], and Gudipati et al. [44] have previously performed polarization spectroscopic investigations of the electronic transitions of DPE. An investigation of the 4,4′-dimethyl derivative was carried out by Yogev and Margulies [45]. Tanizaki et al. [42] investigated the LD of the bands A and B in the near UV region using samples of DPE aligned in stretched poly(vinyl alcohol) (PVA). Gudipati et al. [44] performed photo-selection experiments with synchrotron radiation on matrix-isolated DPE, including also the higher bands C and D. Uznanski et al. [43] considered the bands A and B for DPE aligned in stretched PE, applying an approach similar to the one used in the present study.

On the basis of a careful analysis of UV and IR polarization data Uznanski et al. [43] determined the orientation factors $(K_x, K_y, K_z) = (0.70,\ 0.17,\ 0.13)$ for the three molecular axes of DPE partially aligned in stretched PE (adopting the present labeling of the axes). They found that the first strong band A is polarized along the orientation axis x, yielding $K_x = K_A = 0.70$. In the present experiment we obtain $K_A = 0.73$ (Fig. 1), and we shall assume a slightly more efficient molecular alignment in the present PE sample, corresponding to $(K_x, K_y,$

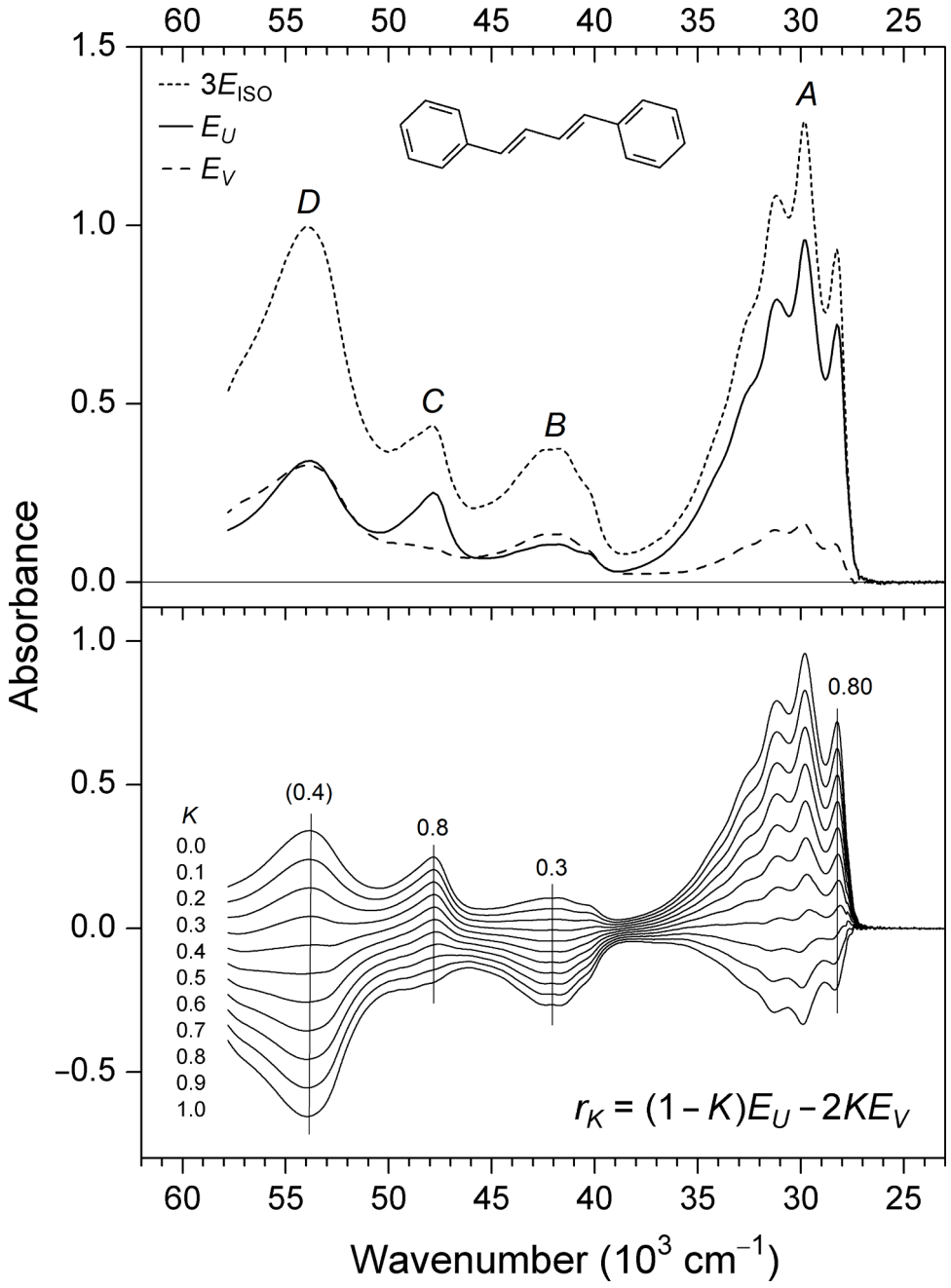

Fig. 2. *Top:* Linear Dichroism (LD) absorbance curves for DPB in stretched polyethylene. E_U and E_V indicate the absorbance curves measured with the stretching direction U parallel and perpendicular to the electric vector of the radiation. $3E_{ISO} = E_U + 2E_V$ is three times the absorbance that would have been measured in an isotropic experiment on the same sample. *Bottom:* Family of reduced absorbance curves $r_K = (1-K)E_U - 2KE_V$ with K varying from 0 to 1 in steps of 0.1.

$K_z) = (0.73,\ 0.15,\ 0.12)$. The moment angles $|\phi_i|$ estimated from Eq. (2) with $K_x = 0.73$ and $K_y = 0.15$ are listed in Table 1. With $K_B = 0.40$ we derive $|\phi_B| = 49$. This is in close agreement with the result of Uznanski et al. [43]. Tanizaki et al. [42] and Gudipati et al. [44] obtained similar results for band *A*, but derived a somewhat larger moment angle for band *B*, $|\phi_B| \approx 65°$.

With K_C close to 0.7 we have $|\phi_C| \approx 0°$ for band *C*, indicating an essentially long axis-polarized transition. The $|\phi_C|$ value derived by Gudipati et al. was close to 21° [44]. The peak *D* in the vacuum UV region has a *K* value around 0.2, suggesting predominantly short axis-polarized absorbance, in reasonable consistency with the results of Gudipati et al. [44]. These authors observed an additional band *E* towards higher wavenumbers, outside the region investigated in the present work.

4.1.2. *Transition moment angles for DPB*

Tanizaki et al. [42] and Kawski and Gryczyński [46,47] investigated samples of DPB aligned in stretched PVA. Tanizaki et al. investigated the LD of bands *A* and *B*, while Kawski and Gryczyński studied the emission and absorption anisotropies of band *A*. Hansen et al. [32] performed an IR polarization spectroscopic investigation of DPB in a thick sample of stretched PE. These authors obtained the orientation factors $(K_x, K_y, K_z) = (\sim 0.55,\ \sim 0.25,\ 0.17)$. In the present experiment using a thin PE sample the molecular alignment is much more efficient, as evidenced by the large *K* equal to 0.80 observed for band *A* (Fig. 2). Similar to previous workers [42,46,47] we shall assume that band *A* is polarized along the molecular orientation axis *x*, yielding $K_x = K_A = 0.80$. We shall further assume that the orientation distribution of DPB in the present stretched PE sample is effectively "rod-like", $K_x \gg K_y = K_z$ [10,11],

Table 1
Observed spectral features and calculated electronic transitions for (*E*)−1,2-diphenylethene (*trans*-stilbene, DPE).

Experimental					LCOAO					
	$\tilde{\nu}$ [a]	$3E_{ISO}$ [b]	K [c]	$\|\phi\|$ [d]	Term [e]	$\tilde{\nu}$ [a]	f [f]	ϕ [d]	B[g]	Leading configurations [h]
A	32.1	1.34	0.73	(0°)	1^1B_u	31.7	**1.37**	(0°)	+0.47	98% [$4a_u \rightarrow 4b_g$]
					2^1B_u	35.9	0.01	+19°	–0.49	42% [$4a_u \rightarrow 5b_g$], 36% [$3a_u \rightarrow 4b_g$]
					2^1A_g	36.0	0	–	0	42% [$4a_u \rightarrow 5a_u$], 34% [$3b_g \rightarrow 4b_g$]
					3^1A_g	44.3	0	–	0	80% [$4a_u \rightarrow 6a_u$], 10% [$2b_g \rightarrow 4b_g$]
					4^1A_g	45.3	0	–	0	50% [$2b_g \rightarrow 4b_g$], 26% [$3b_g \rightarrow 4b_g$]
B	43.1	0.72	0.40	49°	3^1B_u	46.7	**0.74**	+67°	+0.56	50% [$3a_u \rightarrow 4b_g$], 47% [$4a_u \rightarrow 5b_g$]
					5^1A_g	46.8	0	–	0	32% [$1b_g \rightarrow 5b_g$], 27% [$3b_g \rightarrow 4b_g$]
C	49.3	0.88	0.7	0°	4^1B_u	51.7	**0.62**	–1°	+0.84	41% [$3a_u \rightarrow 5b_g$], 38% [$3b_g \rightarrow 5a_u$]
					5^1B_u	54.5	0.03	–24°	+0.24	28% [$4a_u \rightarrow 6b_g$], 23%[$2a_u \rightarrow 4b_g$]
					6^1A_g	54.6	0	–	0	33% [$3a_u \rightarrow 6a_u$], 26% [$2b_g \rightarrow 5b_g$]
					6^1B_u	54.7	0.01	–69°	–0.98	26% [$4a_u \rightarrow 6b_g$], 18% [$3b_g \rightarrow 6a_u$]
					7^1A_g	55.5	0	–	0	41% [$3a_u \rightarrow 5a_u$], 38% [$3b_g \rightarrow 5b_g$]
					8^1A_g	59.7	0	–	0	48% [$2b_g \rightarrow 5b_g$], 41% [$3a_u \rightarrow 6a_u$]
D	56.6	1.52	(0.2)	(73°)	7^1B_u	60.0	**1.07**	+70°	+6.42	43% [$1a_u \rightarrow 5b_g$], 37% [$3b_g \rightarrow 6a_u$]
					8^1B_u	61.2	**0.87**	–34°	–6.34	60% [$2b_g \rightarrow 6a_u$], 11% [$2a_u \rightarrow 4b_g$]
					9^1A_g	63.1	0	–	0	49% [$3b_g \rightarrow 5b_g$], 49% [$3a_u \rightarrow 5a_u$]
					9^1B_u	63.1	10^{-3}	–52°	+0.03	50% [$3a_u \rightarrow 5b_g$], 45% [$3b_g \rightarrow 5a_u$]
					10^1B_u	63.3	**0.39**	–80°	–0.43	40% [$2a_u \rightarrow 4b_g$], 27% [$2b_g \rightarrow 6a_u$]

[a] Peak wavenumber in 1000 cm^{-1}.
[b] $3E_{ISO} = E_U + 2E_V$ (Fig. 1, top).
[c] Orientation factor (Section 4.1).
[d] In-plane transition moment angle (Scheme 2).
[e] 18 lowest terms, full listing provided as S6.
[f] Oscillator strength.
[g] MCD B-term in 10^{-3} β_e D^2/cm^{-1} (β_e = Bohr magneton, D = Debye).
[h] MO surface diagrams are shown in Fig. 5.

Table 2
Observed spectral features and calculated electronic transitions for (*E,E'*)−1,4-diphenyl-1,3-butadiene (DPB).

Experimental					LCOAO					
	$\tilde{\nu}$ [a]	$3E_{ISO}$ [b]	K [c]	$\|\phi\|$ [d]	Term [e]	$\tilde{\nu}$ [a]	f [f]	ϕ [d]	B [g]	Leading configurations [h]
A	29.9	1.29	0.80	(0°)	1^1B_u	28.7	**1.92**	(0°)	+0.32	97% [$4b_g \rightarrow 5a_u$]
					2^1A_g	35.6	0	–	0	36% [$4b_g \rightarrow 6b_g$], 30% [$3a_u \rightarrow 5a_u$]
					2^1B_u	35.6	$3{\cdot}10^{-3}$	+29°	–0.30	38% [$4b_g \rightarrow 6a_u$], 31% [$3b_g \rightarrow 5a_u$]
					3^1A_g	39.8	0	–	0	77% [$4b_g \rightarrow 5b_g$], 12% [$4a_u \rightarrow 5a_u$]
					4^1A_g	41.2	0	–	0	80% [$4a_u \rightarrow 5a_u$], 13% [$4b_g \rightarrow 5b_g$]
B	41.7	0.38	0.3	58°	3^1B_u	45.3	**0.61**	+62°	+0.50	49% [$3b_g \rightarrow 5a_u$], 46% [$4b_g \rightarrow 6a_u$]
					5^1A_g	45.3	0	–	0	48% [$3a_u \rightarrow 5a_u$], 46% [$4b_g \rightarrow 6b_g$]
					4^1B_u	48.7	0.05	+31°	+0.83	67% [$4b_g \rightarrow 7a_u$], 20% [$2b_g \rightarrow 5a_u$]
C	47.8	0.44	0.8	0°	5^1B_u	50.1	**0.21**	+9°	–0.79	33% [$2b_g \rightarrow 5a_u$], 23%[$3b_g \rightarrow 6a_u$]
					6^1A_g	52.5	0	–	0	21% [$4a_u \rightarrow 6a_u$], 19% [$3b_g \rightarrow 5b_g$]
					6^1B_u	52.5	$2{\cdot}10^{-3}$	+2°	+0.09	22% [$3a_u \rightarrow 5b_g$], 22% [$4a_u \rightarrow 6b_g$]
					7^1A_g	53.6	0	–	0	42% [$3a_u \rightarrow 6a_u$], 38% [$3b_g \rightarrow 6b_g$]
					8^1A_g	56.3	0	–	0	60% [$4b_g \rightarrow 7b_g$], 28% [$2a_u \rightarrow 5a_u$]
					7^1B_u	56.8	**0.34**	–44°	+2.09	73% [$4a_u \rightarrow 5b_g$], 6% [$3a_u \rightarrow 6b_g$]
D	54.1	1.00	(0.4)	(50°)	8^1B_u	57.6	**0.78**	–14°	+2.57	28% [$2b_g \rightarrow 5a_u$], 19% [$4b_g \rightarrow 7a_u$]
					9^1A_g	58.1	0	–	0	44% [$3a_u \rightarrow 6a_u$], 40% [$3b_g \rightarrow 5b_g$]
					9^1B_u	58.6	**1.36**	+78°	–4.27	35% [$4a_u \rightarrow 6b_g$], 30% [$3a_u \rightarrow 5b_g$]
					10^1A_g	63.1	0	–	0	37% [$4a_u \rightarrow 7a_u$], 32% [$2b_g \rightarrow 5b_g$]

[a] Peak wavenumber in 1000 cm^{-1}.
[b] $3E_{ISO} = E_U + 2E_V$ (Fig. 2, top).
[c] Orientation factor (Section 4.1).
[d] In-plane transition moment angle (Scheme 2).
[e] 18 lowest terms, full listing provided as S7.
[f] Oscillator strength.
[g] MCD B-term in 10^{-3} β_e D^2/cm^{-1} (β_e = Bohr magneton, D = Debye).
[h] MO surface diagrams are shown in Fig. 5.

consistent with the elongated shape of the molecule: $(K_x,K_y,K_z) = (0.80, 0.10, 0.10)$. The moment angles $|\phi_i|$ estimated from Eq. (2) with $K_x = 0.80$ and $K_y = 0.10$ are listed in Table 2. Like in the case of DPE, the bands *A* and *C* are essentially long axis-polarized, while the polarization directions of bands *B* and *D* deviate significantly from this axis. The results are consistent with those previously obtained for bands *A* and *B* by Tanizaki et al. [42] and for band *A* by Kawski and Gryczyński [46, 47].

4.2. Electronic transitions

4.2.1. Calculated transitions

The 18 lowest transitions for DPE and DPB predicted with LCOAO are listed in Tables 1 and 2, complete listings are provided as S6 and S7. The transitions obtained with TD–CAM-B3LYP/AUG-cc-pVTZ are provided as S11 and S12. Convolutions of the predicted transitions were performed by assigning a Gaussian function to each excitation wavenumber

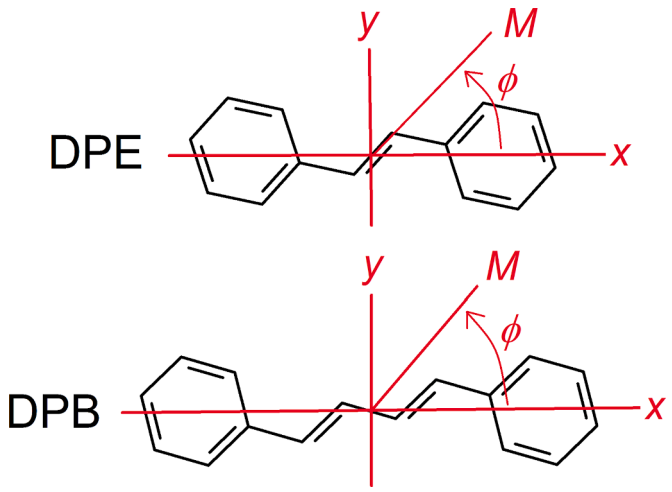

Scheme 2. Definition of in-plane axes and transition moment angles for DPE and DPB (see text).

with an area proportional to the oscillator strength of that transition, using a constant standard deviation, σ = 1500 cm^{-1}. Results obtained with LCOAO, TD–CAM-B3LYP/cc-pVTZ, and TD–CAM-B3LYP/AUG-cc-pVTZ are compared in S2 and S3. In the convolutions shown in Figs. 3 and 4, components corresponding to the absorbance of *U*- and *V*-polarized radiation are indicated. The components were obtained by multiplication of the oscillator strength by the pertinent orientation factors according to Eq. (1): K_i for *U*-polarized and 1 /2 (1 − K_i)) for *V*-polarized radiation. The K_i values were derived from the theoretically predicted moment angles ϕ_i by using the relation

$$K_i = \left(K_x + K_y \tan^2\phi_i\right) / \left(1 + \tan^2\phi_i\right) \quad (3)$$

with (K_x, K_y) equal to $(0.73,\ 0.15)$ for DPE and $(0.80,\ 0.10)$ for DPB.

4.2.2. Assignment of electronic transitions for DPE

The very strong band *A* has an onset at 30,600 cm^{-1} (327 nm) and a maximum at 32,100 cm^{-1} (312 nm) (Fig. 1, Table 1). The transition must be assigned to the 1^1B_u state predicted by LCOAO at 31,700 cm^{-1} (315 nm). It is well described by the HOMO-LUMO excitation, $4a_u \rightarrow 4b_g$ (Fig. 5), and is polarized along the long axis *x* (Scheme 2). Similar results are obtained with TD–CAM-B3LYP (S11).

The next band *B* with onset at 41,700 cm^{-1} (240 nm) and maximum at 43,100 cm^{-1} (232 nm) can be assigned to the 3^1B_u state computed by LCOAO at 46,700 cm^{-1} (214 nm). This transition is essentially due to the promotions $3a_u \rightarrow 4b_g$ and $4a_u \rightarrow 5b_g$ (SHOMO-LUMO and HOMO-SLUMO). The computed moment angle is $\phi = +67°$, indicating a polarization direction deviating significantly from the long axis. The positive sign agrees with previous predictions [42–44], but the numerical value obtained with LCOAO is 18° larger than the experimental estimate, $|\phi| = 49°$ (Table 1). The TD–CAM-B3LYP calculation predicts $\phi = +49°$ (S11), in excellent agreement with the present experimental evidence. On the other hand, the LCOAO result $\phi = +67°$ agrees with the value $|\phi| \approx 65°$ obtained for band *B* by Gudipati et al. [44].

Band *C* with maximum at 49,300 cm^{-1} (203 nm) can be assigned to the 4^1B_u state predicted by LCOAO at 51,700 cm^{-1} (193 nm) (Table 1). This transition is primarily due to the promotions $3a_u \rightarrow 5b_g$ and $3b_g \rightarrow 5a_u$, thus involving the orbitals next to the frontier region (Fig. 5). It is predicted to be long axis-polarized ($\phi = -1°$), in agreement with the experimental moment angle. Similar results are obtained with TD–CAM-B3LYP (S11).

The intense band *D* peaking at 56,600 cm^{-1} (177 nm) in the vacuum UV region is predominantly short axis-polarized. It is predicted to be due to several overlapping transitions, such as 7^1B_u, 8^1B_u, and 10^1B_u predicted by LCOAO with moment angles +70°, −34°, and −80° (Table 1). The resulting convolutions are shown in Fig. 3 (top). However, calculation of electronic states in the high-wavenumber region is problematic. The LCOAO and TD–CAM-B3LYP results differ significantly (Fig. 3), and those obtained with TD–CAM-B3LYP depend on whether diffuse functions are included in the basis set (S2). With diffuse basis functions, CAM-B3LYP computes relatively low-energy virtual π-type MOs with significant non-valence character (S8), thereby complicating the predicted spectrum in the high-wavenumber region.

As discussed by Improta et al. [48] and Angeli et al. [49], the nature of the two lowest ^1B_u states of DPE has been a matter of controversy. LCOAO and TD–CAM-B3LYP predict the 2^1B_u state at 35,900 cm^{-1} (279 nm) and 39,900 cm^{-1} (251 nm), respectively (Tables 1, S11). The leading configurations are $4a_u \rightarrow 5b_g$ and $3a_u \rightarrow 4b_g$, similar to the 3^1B_u state giving rise to band *B*. The 2^1B_u and 3^1B_u states are essentially *minus* and *plus* combinations of the two configurations, a consequence of the approximate pairing symmetry [50] of the DPE π-system. Due to the *minus* character, transition to the 2^1B_u state is predicted to be weak ("parity forbidden"). The analysis of the polarization spectrum of 4, 4′-dimethyl-DPE by Yogev and Margulies [45] indicated a fairly intense, short axis-polarized feature close to 32,400 cm^{-1} (310 nm) which might be due to the 2^1B_u state. But the transition predicted for DPE is essentially long axis-polarized (Tables 1, S11) and it is likely to be buried under the tail of the strong, long axis-polarized absorbance due to the 1^1B_u state (band *A*). The transition may possibly be observed directly in the MCD spectrum of DPE, since positive and negative B-terms are predicted for 1^1B_u and 2^1B_u (Tables 1, S5).

The calculations predict a number of additional ^1B_u states, which are optically weak and not easily observed in the present spectra. The 5^1B_u and 6^1B_u states may provide minor contributions to the absorbance in the region of band *C* (Tables 1, S11). LCOAO predicts relatively large MCD B-terms for these states, and they can possibly be observed by MCD spectroscopy (Tables 1, S3).

4.2.3. Assignment of electronic transitions for DPB

The intense, long axis-polarized band *A* with onset at 28,200 cm^{-1} (355 nm) and maximum at 29,900 cm^{-1} (334 nm) must be assigned to the 1^1B_u state predicted by LCOAO at 28,700 cm^{-1} (348 nm) (Table 2). This state is well described by the HOMO-LUMO excitation, $4b_g \rightarrow 5a_u$ (Fig. 5), and is polarized along the long axis *x* (Scheme 2). Similar results are obtained with TD–CAM-B3LYP (S12).

Band *B* peaking at 41,700 cm^{-1} (240 nm) can be assigned to the 3^1B_u state computed by LCOAO at 45,300 cm^{-1} (221 nm) (Table 2). The experimental moment angle $|\phi| = 58°$ is in good agreement with the angles predicted by LCOAO ($\phi = +62°$) and by TD–CAM-B3LYP ($\phi = +50°$) (S12). The computed 3^1B_u state is due primarily to the configurations $3b_g \rightarrow 5a_u$ and $4b_g \rightarrow 6a_u$, involving promotions similar to those describing the corresponding state of DPE (Fig. 5). The calculated wavenumber of the 3^1B_u state seems to be relatively overestimated, for DPB (Tables 2, S12) as well as for DPE (Tables 1, S11).

Band *C* with a maximum at 47,800 cm^{-1} (209 nm) is long axis-polarized, similar to band *A*. According to LCOAO this band is primarily due to the 5^1B_u state computed at 50,100 cm^{-1} (200 nm) with oscillator strength *f* = 0.21 and moment angle $\phi = +9°$ The 4^1B_u state at 48,700 cm^{-1} (209 nm) is predicted to provide a minor contribution, *f* = 0.05 (Table 2). In contrast, the 4^1B_u and 5^1B_u states computed with TD–CAM-B3LYP at 48,600 and 50,800 cm^{-1} (206 and 197 nm) have similar optical intensities, *f* = 0.15 and 0.16 (S12), resulting in the prediction of a more diffuse nature of band *C* with no well-defined peak in the convolution (Figs. 4, S3). This result depends on the inclusion of diffuse functions in the basis set: With the AUG-cc-pVTZ basis, the calculated 4^1B_u and 5^1B_u states involve promotions to virtual orbitals with large non-valence character, primarily $7a_u$ (S8,S12). The spectrum predicted without inclusion of diffuse functions is more similar to the one obtained with LCOAO (S3), apparently in better agreement with experiment. Additional experimental information may be obtained by MCD spectroscopy, since the B-terms for 4^1B_u and 5^1B_u are predicted by

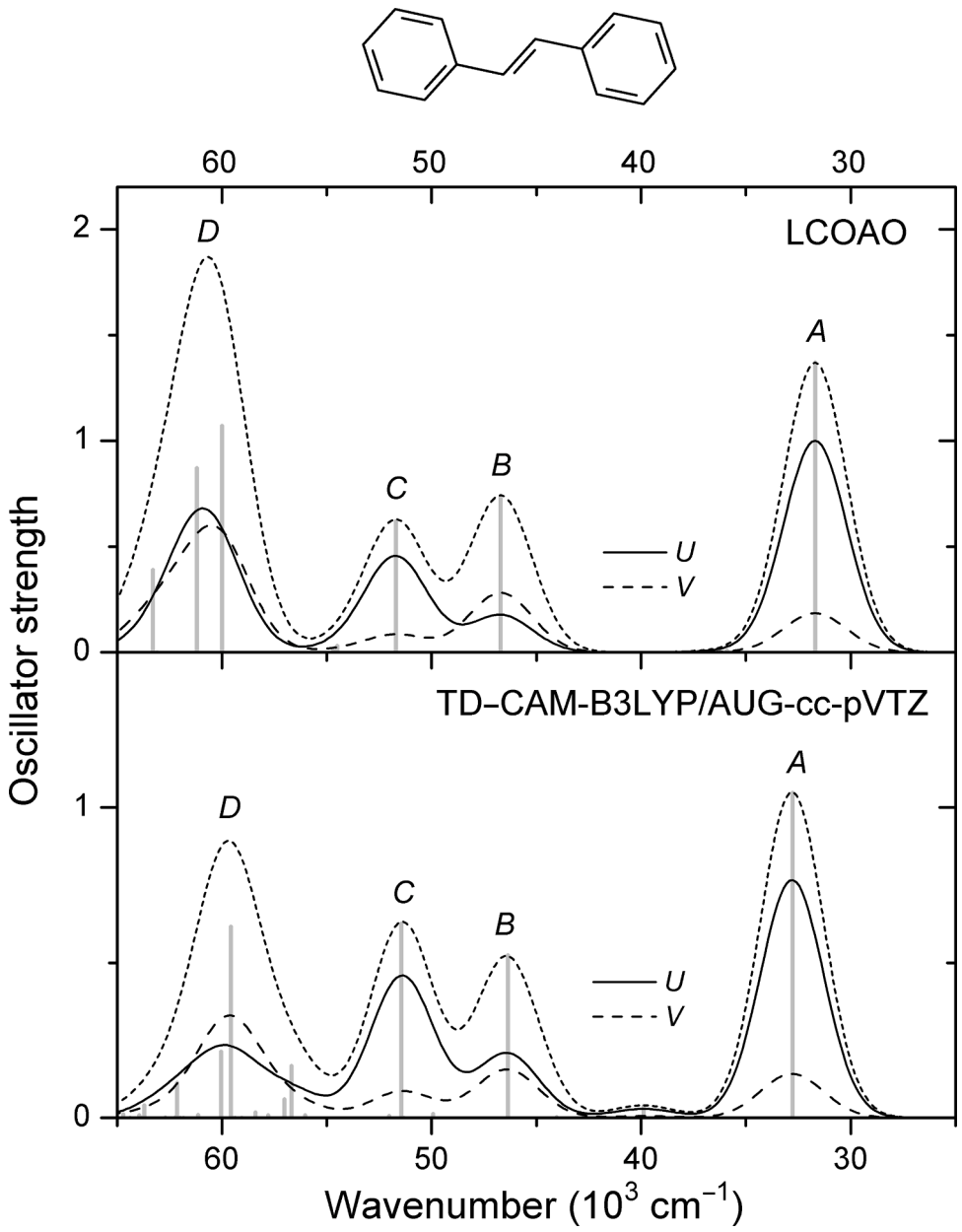

Fig. 3. Gaussian convolutions of calculated electronic transitions for DPE with indication of components corresponding to the absorbance of *U*- and *V*-polarized radiation (Section 4.2.1).

LCOAO to have different signs (Tables 2, S2).

The vacuum UV region exhibits a strong band *D* with a maximum at 54,100 cm^{-1} (185 nm) (Fig. 2). The estimated experimental moment direction deviates considerably from the long axis, $|\phi| \approx 40^{\circ}$ The band is expected to be due to several electronic transitions, such as 7^1B_u, 8^1B_u, and 9^1B_u predicted by LCOAO at 56,800, 57,600, and 58,600 cm^{-1} (176, 174, and 171 nm) with moment angles − 44°, − 14°, and +78° (Table 2). The resulting convolutions are shown in Fig. 4 (top). But as discussed above for DPE, prediction of electronic transitions in this region is not straightforward. Different results are obtained with LCOAO and TD–CAM-B3LYP (Fig. 4), and those with TD–CAM-B3LYP depend on the inclusion of diffuse functions in the basis set (S3). As for DPE, CAM-B3LYP/AUG-cc-pVTZ predicts relatively low-energy virtual MOs with large non-valence character (S8). This leads to the prediction of additional electronic states, but not to an obvious improvement of agreement with experiment.

Several additional ^1B_u states are calculated, which are weak and not easily observed in the present spectra. The 4^1B_u state was mentioned above as a possible contribution to the intensity of band *C*. The 2^1B_u state is predicted by LCOAO (Table 2) to give rise to a weak transition at 35,900 cm^{-1} (279 nm). TD–CAM-B3LYP (S12) computes this state at 39,600 cm^{-1} (253 nm). The predicted transition is nearly long axis-polarized and it is probably hidden under the tail of the strong absorbance due to the 1^1B_u state (band *A*). Like in the case of DPE, transition to the 2^1B_u state may be observed by MCD spectroscopy, since positive and negative B-terms are predicted for the 1^1B_u and 2^1B_u states. A relatively large negative B-term is predicted for the optically weak 6^1B_u state and it may thus be observed in the MCD spectrum (Tables 2, S5).

5. Concluding remarks

The absorbance spectra of DPE and DPB have obvious similarities, characterized by four characteristic bands *A, B, C*, and *D* in the region 58,000–25,000 cm^{-1} (172–400 nm) with similar polarization directions.

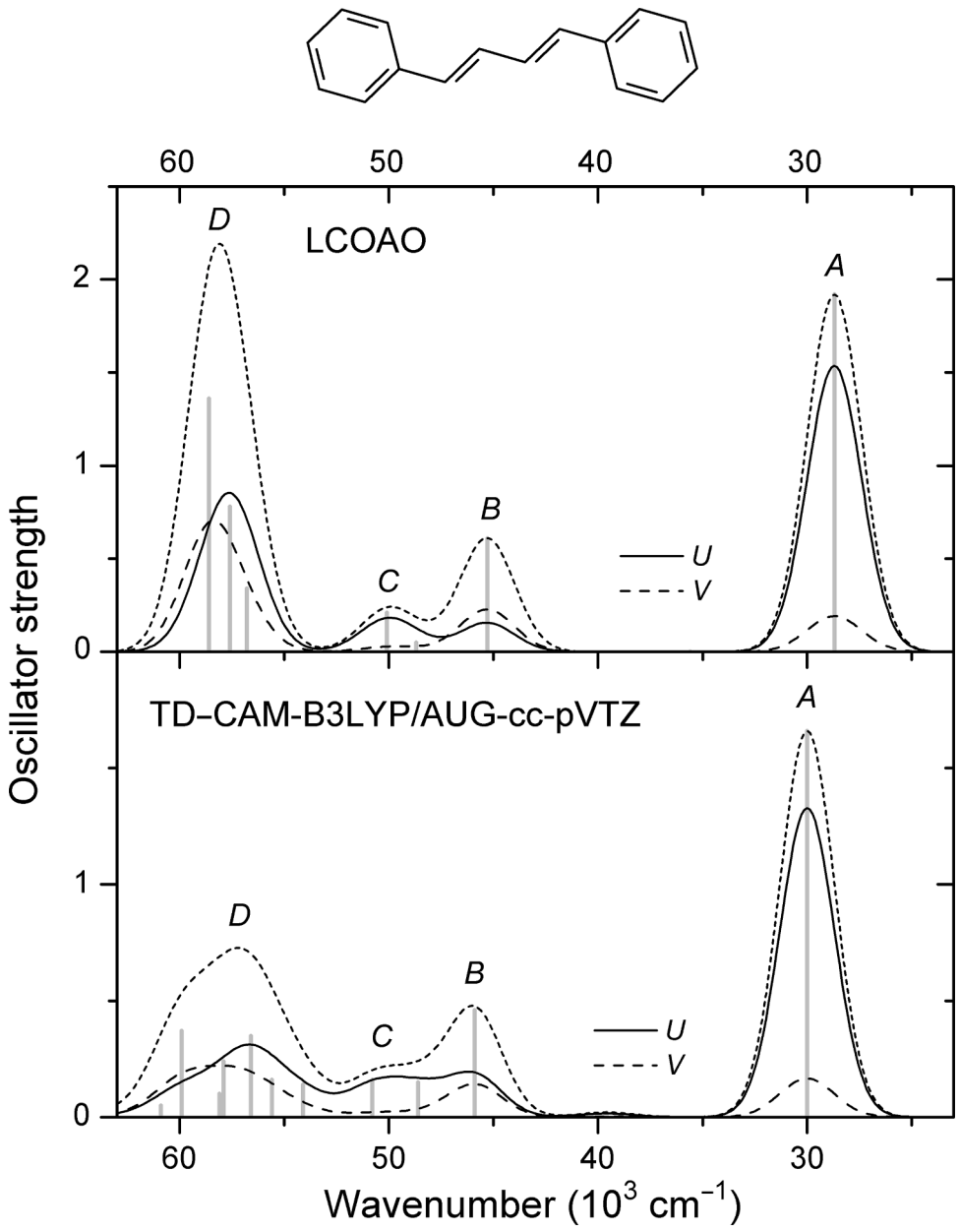

Fig. 4. Gaussian convolutions of calculated electronic transitions for DPB with indication of components corresponding to the absorbance of *U*- and *V*-polarized radiation (Section 4.2.1).

According to the present results, bands *A* and *C* can be characterized as long axis-polarized, while the moment directions of bands *B* and *D* form considerable angles with this axis.

The observed bands *A, B*, and *C* of DPE and their polarization directions are well predicted by calculations using the LCOAO and TD–CAM-B3LYP models. In the case of DPB, the two procedures provide similar results for band *A* and *B*, but differ in the prediction of band *C*. According to LCOAO, this band is predominantly due to one electronic state, while TD–CAM-B3LYP predicts two states in the region of this band with similar optical intensity (this prediction depends on the inclusion of diffuse functions in the basis set). Both theoretical procedures tend to compute band *B* at relatively high wavenumbers, resulting in the prediction band *B* and *C* somewhat too close together. A similar situation was observed for DSB [24].

The prediction of electronic transitions in the region of band *D* in the vacuum UV is difficult. The presently applied theoretical methods differ in the prediction of individual transitions in this region, but the convolutions reproduce quite well the overall appearance of the observed LD spectra.

Several optically allowed transitions are predicted with too low intensity to be observed in the present experimental spectra. The MCD B-terms predicted by LCOAO suggest that some of them may be observed by MCD spectroscopy.

Author contributions

Duy Duc Nguyen conceived and designed the experiments, performed the experiments, analyzed the data, approved the final draft of the paper. *Nykola C. Jones* and *Søren V. Hoffmann* conceived and designed the experiments, performed the experiments, contributed reagents/materials/analysis tools, reviewed drafts of the paper, approved the final draft. *Jens Spanget-Larsen* conceived and designed the experiments, analyzed the data, contributed reagents/materials/analysis tools, prepared figures and tables, performed the computation work, authored

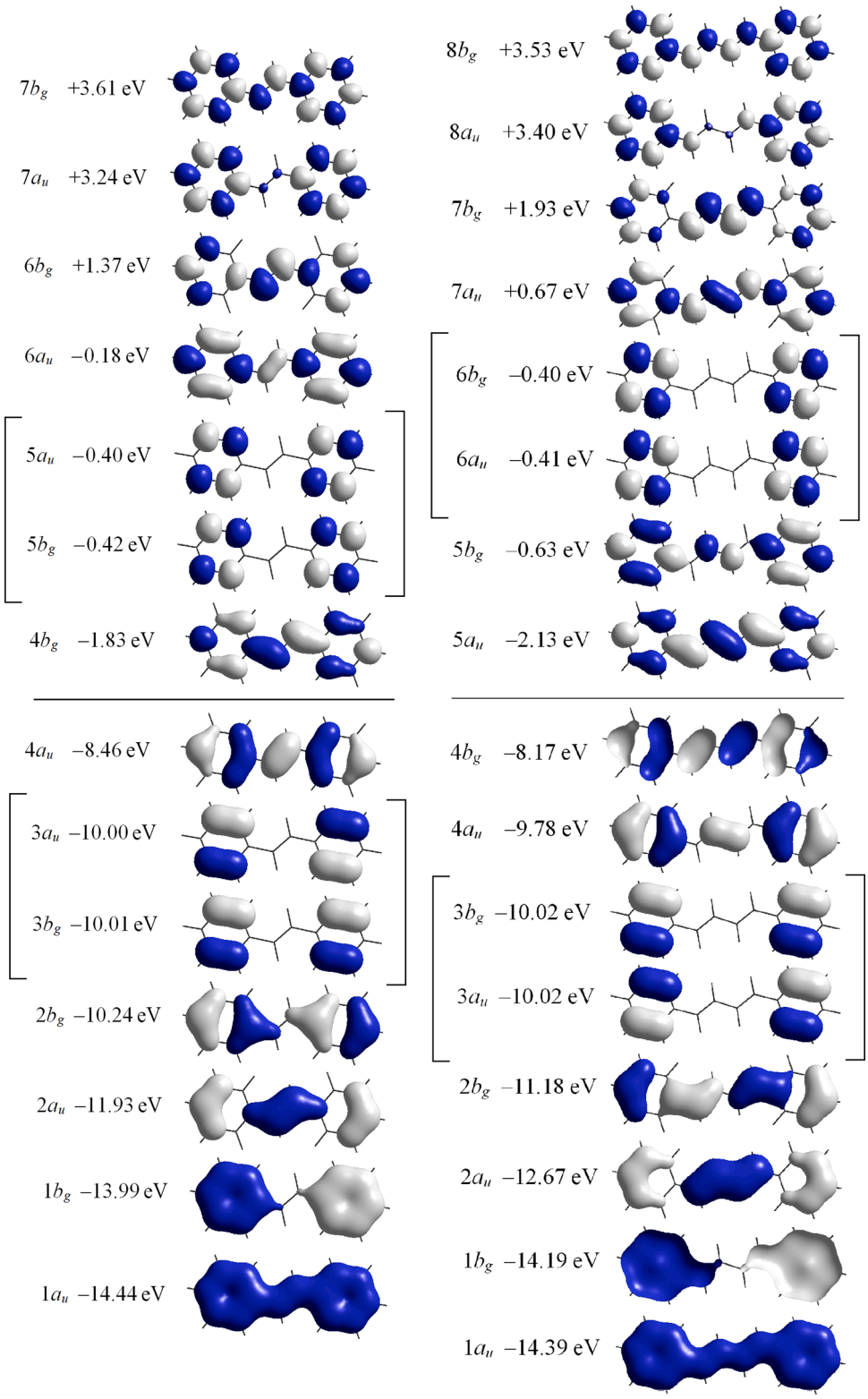

Fig. 5. Energies and symmetries of π type MOs of DPE (left) and DPB (right) computed with LCOAO with indication of orbital amplitudes. MOs obtained with CAM-B3LYP/AUG-cc-pVTZ are provided in S8.

and reviewed drafts of the paper, approved the final draft.

Declaration of Competing Interest

The authors declare that they have no known competing financial interests or personal relationships that could have appeared to influence the work reported in this paper.

Data availability

Spectroscopic data are available from the UV/Vis+ Photochemistry Data Base (https://science-softcon.de/spectra/).

Acknowledgements

This investigation was supported by grants of beam time on the CD1 beamline at ISA. The stay of Nguyen Duc Duy at Roskilde University was enabled by a Ph.D. scholarship granted by the Vietnamese Ministry of Education and Training. The Danish International Development Agency (DANIDA) provided additional support via the Enhancement of Research Capacity (ENRECA) program. The authors are indebted to Søren Møller for a useful discussion and to Eva M. Karlsen for technical assistance.

Supplementary materials

Supplementary material associated with this article can be found, in the online version, at doi:10.1016/j.molstruc.2023.136206.

References

[1] J. Saltiel, J. D'Agostino, E.D. Megarity, L. Metts, K.R. Neuberger, M. Wrighton, O. C. Zafiriou, The *cis-trans* photoisomerization of olefins, Org. Photochem. 3 (1973) 1–113.
[2] M.T. Allen, D.G. Whitten, The photophysics and photochemistry of α,ω-diphenylpolyene singlet states, Chem. Rev. 89 (1989) 1691–1702.
[3] G. Bartolucci, A. Spaletti, U. Mazzucato, Conformational aspects of organic photochemistry, in: J. Waluk (Ed.), Conformational Analysis of Molecules in Excited States, Wiley-VCH, New York, 2000, pp. 237–296. Chapter 5.
[4] J. Catalan, C. Diaz-Oliva, J.C. del Valle, On the first electronic transitions in molecular spectra of conjugated diphenylpolyenes: a reappraisal, Chem. Phys. 525 (2019), 110422.
[5] O.A. Krohn, M. Quick, S.M. Sudarkova, I.N. Ioffe, C. Richter, S.A. Kovalenko, Photoisomerization dynamics of *trans-trans, cis-trans*, and *cis-cis* diphenylbutadiene from broadband transient absorption spectroscopy and calculations, J. Chem. Phys. 152 (2020), 224305.
[6] N. Karmakar, M. Das, Low-lying excited states of diphenylpolyenes and its derivatives in singlet fission: a density matrix renormalization group study, Comput. Theor. Chem. 1217 (2022), 113918.
[7] T. Knežević, J. Biswas, B. Datta, DFT and TD-DFT computational investigations of diphenyl polyene derivatives for optoelectronic application, Bull. Mater. Sci. 45 (2022) 223.
[8] A.J. Miles, S.V. Hoffmann, Y. Tao, R.W. Janes, B.A. Wallace, Synchrotron radiation circular dichroism (SRCD) spectroscopy: new beamlines and new applications in biology, Spectroscopy 21 (2007) 245–255.
[9] A.J. Miles, R.W. Janes, A. Brown, D.T. Clarke, J.C. Sutherland, Y. Tao, B. A. Wallace, S.V. Hoffmann, Light flux density threshold at which protein denaturation is induced by synchrotron radiation circular dichroism beamlines, J. Synchrotron Radiat. 15 (2008) 420–422.
[10] J. Michl, E.W. Thulstrup, Spectroscopy with Polarized Light. Solute alignment by photoselection in Liquid crystals, Polymers and Membranes, VCH-Wiley, Deerfield Beach, FL, 1986, p. 1995.
[11] E.W. Thulstrup, J. Michl, Elementary Polarization Spectroscopy, Wiley-VCH, New York, Weinheim, 1989.
[12] F. Madsen, I. Terpager, K. Olskær, J. Spanget-Larsen, Ultraviolet-visible and infrared linear dichroism spectroscopy of 1,8-dihydroxy-9,10-anthraquinone aligned in stretched polyethylene, Chem. Phys. 165 (1992) 351–360.
[13] A. Rodger, B. Nordén, Circular Dichroism and Linear Dichroism, Oxford University Press, UK, 1997.
[14] B. Nordén, A. Rodger, T. Dafforn, Linear Dichroism and Circular Dichroism: A Textbook on Polarized-Light Spectroscopy, RCS Publishing, Cambridge, UK, 2010.
[15] E.W. Thulstrup, J. Waluk, J. Spanget-Larsen, Electronic spectroscopy: linear dichroism, applications, in: J.C. Lindon, G.E. Tranter, D.W. Koppenaal (Eds.), Encyclopedia of Spectroscopy and Spectrometry, 3rd ed., Academic Press, Oxford, UK, 2017, pp. 595–600.
[16] J. Spanget-Larsen, The alternant hydrocarbon pairing theorem and all-valence electrons theory. an approximate LCOAO theory for the electronic absorption and MCD spectra of conjugated organic compounds. 1, Croat. Chem. Acta 59 (1986) 711–717.
[17] J. Spanget-Larsen, The alternant hydrocarbon pairing theorem and all-valence electrons theory. An approximate LCOAO theory for the electronic absorption and MCD spectra of conjugated organic compounds. 2, Theor. Chem. Acc. 98 (1997) 137–153.
[18] S. Grimme, Calculation of the electronic spectra of large molecules, Rev. Comput. Chem. 20 (2004) 153–218.
[19] M.E. Casida, Review: time-dependent density-functional theory for molecules and molecular solids, J. Mol. Struct. THEOCHEM 914 (2009) 3–18.
[20] C. Adamo, D. Jacquemin, The calculations of excited-state properties with time-dependent density functional theory, Chem. Soc. Rev. 42 (3) (2013) 845–856.
[21] J.B. Foresman, Æ. Frisch, Exploring Chemistry with Electronic Structure Methods, 3rd ed., Gaussian Inc, Wallingford CT, 2015.
[22] T. Yanai, D. Tew, N.A. Handy, New hybrid exchange-correlation functional using the Coulomb-attenuating method (CAM-B3LYP), Chem. Phys. Lett. 393 (2004) 51–57.
[23] J. Michl, Magnetic circular dichroism of aromatic molecules, Tetrahedron 40 (1984) 3845–3934.
[24] D.D. Nguyen, N.C. Jones, S.V. Hoffmann, J. Spanget-Larsen, Near and vacuum UV polarization spectroscopy of 1,4-distyrylbenzene, Spectrochim. Acta A 286 (2023), 122019.
[25] PhotochemCAD: https://omlc.org/spectra/PhotochemCAD/html/110.html, https://omlc.org/spectra/PhotochemCAD/html/115.html (accessed 13 September 2022).
[26] J. Spanget-Larsen, LCOAO computer program: FORTRAN source code with sample input and output. ResearchGate (2014). 10.13140/2.1.3455.6482.
[27] M.J. Frisch, G.W. Trucks, H.B. Schlegel, G.E. Scuseria, M.A. Robb, J.R. Cheeseman, G. Scalmani, V. Barone, G.A. Petersson, H. Nakatsuji, X. Li, M. Caricato, A. V. Marenich, J. Bloino, B.G. Janesko, R. Gomperts, B. Mennucci, H.P. Hratchian, J. V. Ortiz, A.F. Izmaylov, J.L. Sonnenberg, D. Williams-Young, F. Ding, F. Lipparini, F. Egidi, J. Goings, B. Peng, A. Petrone, T. Henderson, D. Ranasinghe, V. G. Zakrzewski, J. Gao, N. Rega, G. Zheng, W. Liang, M. Hada, M. Ehara, K. Toyota, R. Fukuda, J. Hasegawa, M. Ishida, T. Nakajima, Y. Honda, O. Kitao, H. Nakai, T. Vreven, K. Throssell, J.A. Montgomery Jr., J.E. Peralta, F. Ogliaro, M. J. Bearpark, J.J. Heyd, E.N. Brothers, K.N. Kudin, V.N. Staroverov, T.A. Keith, R. Kobayashi, J. Normand, K. Raghavachari, A.P. Rendell, J.C. Burant, S.S. Iyengar, J. Tomasi, M. Cossi, J.M. Millam, M. Klene, C. Adamo, R. Cammi, J.W. Ochterski, R.L. Martin, K. Morokuma, O. Farkas, J.B. Foresman, D.J. Fox, Gaussian 16, Revision A.03, Gaussian, Inc., Wallingford CT, 2016.
[28] A.D. Becke, Density-functional thermochemistry. III. The role of exact exchange, J. Chem. Phys. 98 (1993) 5648–5652.
[29] C. Lee, W. Yang, R.G. Parr, Development of the Colle-Salvetti correlation-energy formula into a functional of the electron density, Phys. Rev. B Condens. Matter Mater. Phys. 37 (1988) 785–789.
[30] T.H. Dunning Jr, Gaussian basis sets for use in correlated molecular calculations. I. The atoms boron through neon and hydrogen, J. Chem. Phys. 90 (1989) 1007–1023.
[31] R.A. Kendall, T.H. Dunning Jr, R.J. Harrison, Electron affinities of the first-row atoms revisited. Systematic basis sets and wave functions, J. Chem. Phys. 96 (1992) 6796–6806.
[32] B.K.V. Hansen, S. Møller, J. Spanget-Larsen, The vibrational structure of (*E,E'*)-1,4-diphenyl-1,3-butadiene. Linear dichroism FT-IR spectroscopy and quantum chemical calculations, Spectrochim. Acta A 65 (2006) 770–778.
[33] S. Miertuš, E. Scrocco, J. Tomasi, Electrostatic interaction of a solute with a continuum. A direct utilizaion of AB initio molecular potentials for the prevision of solvent effects, Chem. Phys. 55 (1981) 117–129.
[34] J. Tomasi, M. Persico, Molecular interactions in solution: an overview of methods based on continuous distributions of the solvent, Chem. Rev. 94 (1994) 2027–2094.
[35] C.J. Cramer, D.G. Truhlar, Implicit solvation models: equilibria, structure, spectra, and dynamics, Chem. Rev. 99 (1999) 2161–2200.
[36] G. Scalmani, M.J. Frisch, Continuous surface charge polarizable continuum models of solvation. I. General formalism, J. Chem. Phys. 132 (2010), 114110.
[37] S. Grimme, S. Ehrlich, L. Goerigk, Effect of the damping function in dispersion corrected density functional theory, J. Comput. Chem. 32 (2011) 1456–1465.
[38] M. Levitus, K. Schmieder, H. Ricks, K.D. Shimizu, U.H.F. Bunz, M.A. Garcia-Garibay, Steps to demarcate the effects of chromophore aggregation and planarization in poly(phenyleneethynylene)s. 1. Rotationally interrupted conjugation in the excited states of 1,4-bis(phenylethynyl)benzene, J. Am. Chem. Soc. 123 (18) (2001) 4259–4265.
[39] M. Levitus, M.A. Garcia-Garibay, Polarized electronic spectroscopy and photophysical properties of 9,10-bis(phenylethynyl)anthracene, J. Phys. Chem. A 104 (38) (2000) 8632–8637.
[40] D.D. Nguyen, N.C. Jones, S.V. Hoffmann, S.H. Andersen, P.W. Thulstrup, J. Spanget-Larsen, Electronic states of 1,4-bis(phenylethynyl)benzene: a synchrotron radiation linear dichroism investigation, Chem. Phys. 392 (2012) 130–135.
[41] P.W. Thulstrup, N.C. Jones, S.V. Hoffmann, J. Spanget-Larsen, Electronic states of the fluorophore 9,10-bis(phenylethynyl)anthracene (BPEA). A synchrotron radiation linear dichroism investigation, Chem. Phys. Lett. 559 (2013) 35–40.
[42] Y. Tanizaki, H. Inoue, T. Hoshi, J. Shiraishi, Localized and delocalized electronic transitions in diphenylacetylene, stilbene and diphenylbutadiene, Z. Phys. Chem. 74 (1971) 45–58 (N. F.).
[43] P. Uznanski, M. Kryszewski, E.W. Thulstrup, Polarized absorption spectroscopy of *trans*-azobenzene and *trans*-stilbene in stretched polyethylene, Spectrochim. Acta A 46 (1990) 23–27.
[44] M.S. Gutipati, M. Maus, J. Daverkausen, G. Hohlneicher, Higher excited states of aromatic hydrocarbons. III. Assigning the in-plane polarized transitions in low-symmetry molecules: chrysene and E-stilbene, Chem. Phys. 192 (1995) 37–47.
[45] A. Yogev, L. Margulies, Polarized absorption and emission spectra of, 4,4'-dimethylstilbene, Isr. J. Chem. 16 (1977) 258–263.
[46] A. Kawski, Z. Gryczyński, On the determination of transition-moment directions from emission anisotropy measurements, Z. Naturforsch. 41a (1986) 1195–1199.
[47] A. Kawski, Z. Gryczyński, On the determination of transition-moment directions from absorption anisotropy measurements, Z. Naturforsch. 42 (1987) 617–621.

[48] R. Improta, F. Santoro, C. Dietl, E. Papastathopoulos, G. Gerber, Time dependent DFT investigation of the two lowest ^1B_u states of the *trans* isomer of stilbene and stiff-stilbenes, Chem. Phys. Lett. 387 (2004) 509–516.

[49] C. Angeli, R. Improta, F. Santoro, On the controversial nature of the 1 ^1B_u and 2 ^1B_u states of *trans*-stilbene: the *n*-electron valence state perturbation theory approach, J. Chem. Phys. 130 (2009), 174307.

[50] R. Pariser, Theory of the electronic spectra and structure of the polyacenes and of alternant hydrocarbons, J. Chem. Phys. 24 (1956) 250–268.